

Integrated high-resolution tomography

Marco A. Perez and John C. Bancroft

ABSTRACT

A common problem in seismic tomography is the inadequate amount of data required for accurate traveltimes inversion. The inherent nature in which data is acquired and the subsurface velocities of the survey area can result in a nonuniform distribution of raypaths. In such instances the statistical nature of tomographic inversion biases the solution to reflect the acquisition instead of the geologic properties. This work outlines a method for using the quasi-null space, a measure of inversion reliability, to produce a more constrained solution. In this method, two seismic experiments with different acquisition geometries are used to determine velocity models over the same geologic region. Using the well-constrained portions of the two resulting velocity models, as determined from the quasi-null space, a final tomogram is determined. Testing shows that the combination of two seismic experiments over the same geologic model and null space analysis yield superior tomograms.

INTRODUCTION

Interpreting seismic data in complex structures requires accurate subsurface images, many times obtained only through prestack depth migration. Prestack depth migration inherently requires an accurate velocity model that can be determined via tomography. Tomographic methods use recorded traveltimes for velocity model estimation. An initial velocity model estimate is updated attempting to minimize the error between the modelled and observed traveltimes. It is assumed that the velocity model yielding the minimum residual traveltimes accurately represents the subsurface velocities.

Two different types of tomography are utilized in this work: reflection and transmission. Transmission tomography and in this work consists of crosswell acquisition geometries and deals with purely transmitted signals. The direct traveltimes from source to receiver reveal information of the unknown parameters to be determined: the subsurface velocities of the survey area. Reflection tomography attempts to determine subsurface velocities from a signal that has been undergone reflection at seismologic impedance contrast along its travel path between source and receiver. In this case, recorded traveltimes reveal subsurface velocities as well as reflector positions.

Bishop et al (1985) presented a classic paper outlining the basic theory of seismic reflection tomography. Parameterizing both the velocities and reflector positions as unknown quantities, a final multi-layered velocity function was determined after various iterations of modelling, solving a set of overdetermined equations and model parameter adjustment. Lines and LaFehr (1989) presented the basic theory of transmission tomography using a crosswell experiment. The same inversion process

used in reflection tomography is used in the transmission problem except that only the velocities are parameterized. It has been shown that using transmission or reflection tomography, an accurate velocity model can be constructed.

There is, however, a basic problem in tomography: the lack of data required to properly constrain the inversion. The acquired data inherently consists of an angle-limited distribution of rays because of the nature of the acquisition geometry and velocity anomalies present within the earth. A non-uniform distribution translates into some areas of the subsurface receiving minimal or no ray coverage. Angle-limited acquisition results in the lack of linearly independent data required to resolve the subsurface properties. Both the lack of sufficient ray coverage and linearly independent data results in small singular values which when inverted bias the tomographic result. The consequence is the inability to obtain a unique geologic solution. A number of different techniques have been developed with the goal of improving the resulting velocity model by limiting the effects of the unconstrained parameters. Phillips and Fehler (1991) have given a review of popular regularization methods that emphasise the suppression of small singular values. Carrion (1991) developed a dual method in which the inversion uses both the data and imposed constraints which compensates for the lack of data. Bohm and Versnaver (1999) developed an iterative adaptive grid scheme based on null space identification and the resolution of the resultant velocity model. By modifying the cell size based on the reliability of the inversion, the cell size is increased or decreased so as to maximise both the reliability and resolution of the solution.

The conventional tomographic method of determining subsurface velocities consists in proposing an initial model through which traveltimes are simulated and compared to recorded data. This work follows the same flow using a finite-difference approximation to the eikonal equation to model traveltimes and raypaths (Perez and Bancroft, 2000, Perez and Bancroft, 2001). Minimising the error between the modelled and recorded traveltimes determines velocities of the subsurface geology. However, fitting data traveltimes with the model response is a necessary but not sufficient criterion for finding the correct solution to the traveltime inversion problem. In an attempt to reach a unique solution a modification of the null space identification scheme is used. For a single velocity model, two different sets of data are acquired, each with different acquisition geometry. The ray coverage for the two surveys differs resulting in distinct illumination patterns of the subsurface. The tomographic solution and the null space are computed for each of the surveys. By identifying the better-constrained cells using the null space criterion a more controlled tomogram is ascertained.

THEORY

Tomography

The inversion problem is presented using similar notation to that of Bishop et al (1985). Let x denote the horizontal distance along the earth's surface and let z represent depth. The two-dimensional area of interest is divided into nx by nz square cells, each with a slowness denoted by $s(j)$ numbered from left to right and top to

bottom. There are n reflectors in the model with depths denoted as $z_n(x)$. A column vector \mathbf{m} is constructed containing all of the parameters that describe the model. In transmission tomography, the parameters consist of $(nx \cdot nz)$ velocities from $s(1)$ to $s(nx \cdot nz)$. Reflection tomography requires the number of parameters to be $(nx \cdot nz + n \cdot nx)$, which includes all of the slowness cells and the number of reflectors multiplied by the number of points describing the reflector.

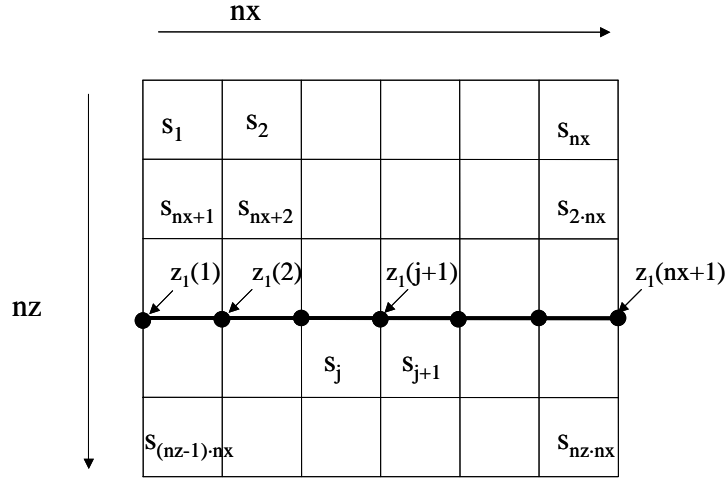


FIG. 1. Schematic diagram illustrating notation used to formulate tomographic problem.

A column vector \mathbf{t} is also constructed, containing the recorded data of the survey. The number of entries in \mathbf{t} is a function of the number of sources (ns), receivers (nr) and reflectors (n) in the model, equivalent to the number of rays (N) that have been recorded.

The mathematical formulation of the tomographic problem is neatly presented in Lines and LaFehr (1989), and is summarized below. The traveltime for the i th ray, t_i , can be thought of as a sum of the distance travelled times the slowness of each of the cells crossed by a given ray.

$$\sum_j d_{ij} m_j = t_i, \quad (1)$$

where d_{ij} is the distance of the i th ray in the j th cell and m_j is the slowness of the j th cell. In matrix notation the traveltime equations can be written succinctly as

$$\mathbf{Dm} = \mathbf{t} \quad (2)$$

where \mathbf{D} , a Jacobian matrix, \mathbf{m} is the slowness vector and \mathbf{t} is the traveltime vector. \mathbf{D} has elements d_{ij} that are the partial derivatives of time with respect to slowness $\left(\frac{\partial t}{\partial s}\right)$, corresponding to the distances travelled by the rays within a cell. Due to Snell's law, in heterogeneous media equation (2) becomes nonlinear in slowness. However, model parameters are computed iteratively by solving linearized equations from some starting model. In full matrix form we have,

$$\begin{bmatrix} d_{11} & d_{12} & \cdot & d_{1-nx} & \cdot & d_{1-nxnz} \\ d_{21} & d_{22} & \cdot & d_{2-nx} & \cdot & d_{2-nxnz} \\ \cdot & \cdot & \cdot & \cdot & \cdot & \cdot \\ \cdot & \cdot & \cdot & \cdot & \cdot & \cdot \\ d_{nznx-1} & d_{nznx-2} & \cdot & d_{nznx-nx} & \cdot & d_{nznx-nznx} \end{bmatrix} \begin{bmatrix} s_1 \\ s_1 \\ \cdot \\ \cdot \\ s_{nz-nx} \end{bmatrix} = \begin{bmatrix} t_1 \\ t_2 \\ \cdot \\ \cdot \\ t_{nz-nx} \end{bmatrix} \quad (3)$$

Since the initial model is usually incorrect it is useful to rewrite equation (2) as

$$D\Delta\mathbf{m} = \Delta\mathbf{t} \quad (4)$$

where $\Delta\mathbf{t}$ is the residual traveltimes, whose components correspond to the difference between the modeled and recorded traveltimes, and $\Delta\mathbf{m}$ is the parameter update vector. The updated slowness solution is given by adding $\Delta\mathbf{m}$ to the original vector \mathbf{m} .

To parameterize the reflector depth, it is included into the Jacobian matrix D and the model vector \mathbf{m} . The partial derivatives of time are taken with respect to the unknown quantity, $\left(\frac{\partial t}{\partial z_n(x)}\right)$, in this case the reflector depth and added into the Jacobian for each ray. This derivative has been computed analytically by Bishop et al (1986) and has the form

$$\frac{\partial t}{\partial z} = 2s_{ij} \cos \beta \cos \theta \left(\frac{x_R - x_{m-1}}{x_m - x_{m-1}} \right) \quad (5)$$

where s_{ij} is the slowness of the cell, β is the angle of the reflector with respect to the horizontal, θ is the angle of incidence of the ray to the reflector, and x_R, x_m, x_{m-1} are points within the cell defining the reflector as shown in Figure 2.

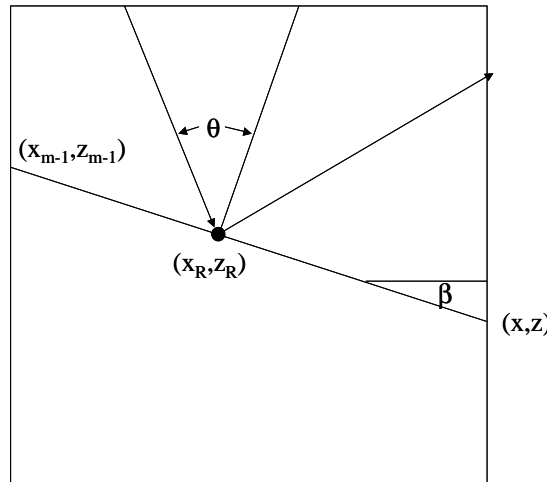


FIG. 2. Schematic diagram of reflector depth derivative.

The resulting matrix equation has the form

$$\begin{bmatrix} d_{11} & \cdot & d_{1-nznx} & z_1(1) & \cdot & z_1(nx) & \cdot & z_n(nx) \\ d_{21} & \cdot & d_{2-nznx} & z_1(1) & \cdot & z_1(nx) & \cdot & z_n(nx) \\ \cdot & \cdot \\ \cdot & \cdot \\ d_{nznx-1} & \cdot & d_{nznx-nznx} & z_1(1) & \cdot & z_1(nx) & \cdot & z_n(nx) \end{bmatrix} \begin{bmatrix} \Delta s_1 \\ \cdot \\ \Delta s_{nznx} \\ \Delta z_1(1) \\ \cdot \\ \Delta z_n(nx) \end{bmatrix} = \begin{bmatrix} \Delta t_1 \\ \Delta t_2 \\ \cdot \\ \Delta t_{nznx} \end{bmatrix} \quad (6)$$

Inverting for the Jacobian matrix yields a solution for parameter adjustment.

Singular Value Decomposition

The basis for solving nonlinear, least-square problems is through iteratively solving linearized equations. Parameters are continuously updated until either a minimal discrepancy level is reached between the model response and the observation, or the change between the updated model and the previous model is minimal. A simple explanation of the technique to be used is given by Lines and Treitel (1984). The linear problem consists of n observations denoted by the vector \mathbf{t} . The model s is a function of p parameters. Letting s^0 be the initial estimate, the initial model response is \mathbf{t}^0 . The residual travelttime errors are then $\Delta \mathbf{t}^0$ and the parameter adjustment values are $\Delta \mathbf{s}$. The initial equation is formulated as

$$\overline{\overline{D}} \Delta \mathbf{s} = \overline{\overline{\Delta \mathbf{t}}} \quad (7)$$

of which the formal solution is

$$\overline{\overline{\Delta \mathbf{s}}} = \overline{\overline{D}}^{-1} \overline{\overline{\Delta \mathbf{t}}}. \quad (8)$$

The difficulty in solving such an equation is that normally, in geophysical applications, the problem is not well posed. The Jacobian matrix, \mathbf{D} , is overdetermined with the number of data points exceeding the number of model parameters. Thus an inverse to \mathbf{D} cannot be found conventionally. A solution can be found however by decomposing \mathbf{D} into three matrices whose product is \mathbf{D} ,

$$\overline{\overline{D}} = \overline{\overline{U}} \overline{\overline{\Lambda}} \overline{\overline{V}}^T. \quad (9)$$

Here \mathbf{U} is an $n \times p$ matrix whose columns contain p of the total n orthonormal observation eigenvectors u_i that satisfy

$$\overline{\overline{D}} \overline{\overline{D}}^T u_i = \lambda_i^2 u_i. \quad (10)$$

\mathbf{V} is a $p \times p$ matrix whose columns contain the p orthonormal parameter eigenvectors that satisfy

$$\overline{\overline{D}}^T \overline{\overline{D}} v_i = \lambda_i^2 v_i. \quad (11)$$

Finally, \mathbf{A} is a $p \times p$ diagonal matrix containing at most p positive singular values that correspond to the positive square roots of the eigenvalues λ_i^2 of $\mathbf{D}^T \mathbf{D}$. The decomposition of \mathbf{D} leads to the use of the Lanczos inverse,

$$\overline{\overline{D}}_L^{-1} = \overline{\overline{V}} \overline{\overline{\Lambda}}^{-1} \overline{\overline{U}}^T, \quad (12)$$

to solve equation (8). The solution becomes

$$\overline{\Delta s} = \overline{\overline{V}} \overline{\overline{\Lambda}}^{-1} \overline{\overline{U}}^T \overline{\Delta t}. \quad (13)$$

Taking a closer look at the solution, written in its expanded form, reveals a weighted vector product sum

$$\overline{\Delta s} = \frac{1}{\lambda_1} v_1 u_1^T \overline{\Delta t} + \frac{1}{\lambda_2} v_2 u_2^T \overline{\Delta t} + \dots + \frac{1}{\lambda_p} v_p u_p^T \overline{\Delta t}. \quad (14)$$

The solution vector is the weighted sum of the p parameter eigenvectors v_i with weights of $\frac{u_i^T \overline{\Delta t}}{\lambda_i}$. Thus if the weight is small then v_i has little influence on the

solution. Also if λ_i is small then the term $\frac{u_i^T \overline{\Delta t}}{\lambda_i}$ will have a great influence on the solution. It is the small singular values λ_i , which are most problematic in inversion problems.

Null space

The null space is defined for matrices that are rank deficient. In such cases there exists a vector \mathbf{u}_0 such that

$$\overline{\overline{D}} \overline{\overline{u}}_0 = 0. \quad (15)$$

With such a matrix \mathbf{D} , and its appropriate vector \mathbf{u}_0 , an infinite number of solutions to equation (7) exist since

$$\overline{\Delta t} = \overline{\overline{D}} (\overline{\Delta s} + \alpha \overline{\overline{u}}_0) = \overline{\overline{D}} \overline{\Delta s} + \alpha \overline{\overline{D}} \overline{\overline{u}}_0 = \overline{\overline{D}} \overline{\Delta s} \quad (16)$$

where α is any real number. When singular value decomposition is performed, a property of the matrix \mathbf{V} is that the columns corresponding to the singular values equal to zero, constitute an orthonormal basis of the null space. Vesnaver (1994) defines the quasi-null singular values as those singular values below a given threshold. The quasi-null space is defined as the sum of squares of the entries columns of \mathbf{V} whose corresponding singular values are above a predefined threshold. This is expressed mathematically as

$$m_i = \sum V_{ij}^2 \quad (17)$$

where only the values above the prescribed threshold are included within the summation. A map of this quasi-null space highlights the cells that are most reliable for traveltimes inversion.

Vesnaver proposed a change in cell size to limit the size of the quasi-null space. Increasing the cell size however reduces the resolution. The method proposed in this work uses two seismic datasets with different acquisition geometries over the same geologic model. Determining the quasi-null space for each, the more reliable cells of each inversion is chosen thus increasing the reliability of the inversion without reducing the resolution.

RESULTS

Three models are used to test the validity of the proposed method: a constant velocity model, a velocity model with a high velocity layer and a model with a high velocity anomaly in the middle. These three velocity models are shown in Figure 3. The background velocity for each is 3000m/s with the high velocity anomalies have a velocity of 3300m/s.

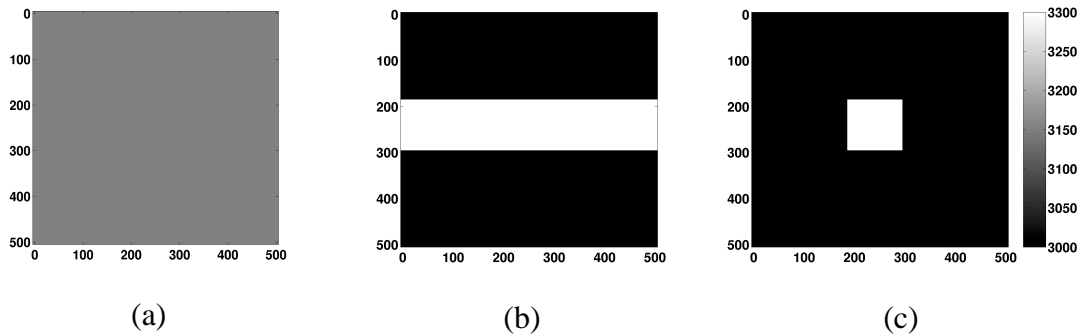


FIG. (3) Three models used to test tomography: model 1 (a), model 2 (b) and model 3 (c).

In the tomographic analysis that follows, a resulting velocity model was obtained by using both reflection and transmission tomography independently. The initial velocity estimate for the constant velocity model was 3300m/s. The two remaining models used an initial velocity estimate of 3000m/s. Three iterations were performed for each tomographic method with smoothing filter applied after each iteration. The two different acquisition geometries used mimic a crosswell and a surface reflection survey. For the crosswell survey the sources were placed vertically at 10m spacing at $x=0$. The receivers were also placed vertically with 10m spacing at $x=500$. Traveltimes were calculated along a 10×10 m grid, while 50×50 m cell sizes were used for inversion.

Transmission tomography

Using transmission tomography, the following results were obtained inverting for model 1. Figure 4 displays the velocity determined after three iterations.

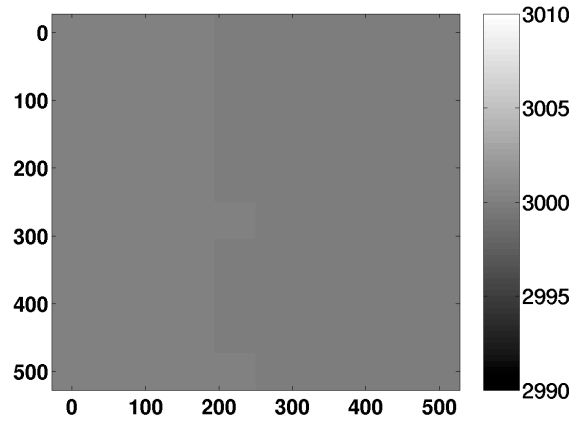


FIG. 4. Transmission tomography inversion result for model 1.

The result is very good with minimal discrepancy between the actual velocity model and the computed one. There is sufficient ray coverage to adequately sample the model. Smoothing the solution after each iteration assists convergence to a constant velocity field.

Figure 5 shows the result in attempting to invert for model 2 after three iterations.

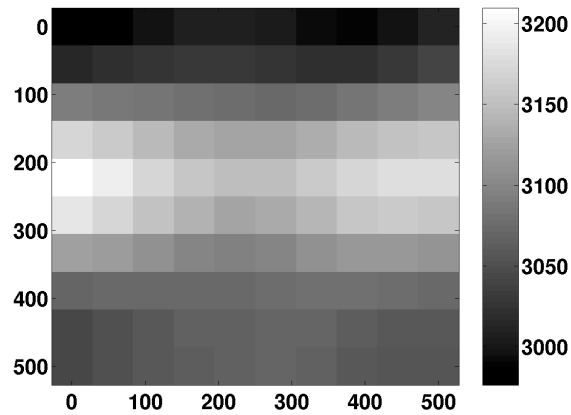


FIG. 5 Transmission tomography inversion result for model 2.

Note that the horizontal high velocity anomaly is present though the boundaries are not resolved in great detail. Thus, since there is a smearing over a larger number of cells, the velocity of the anomaly is less than it should be.

Figure 6 shows the results of the inversion for model 3.

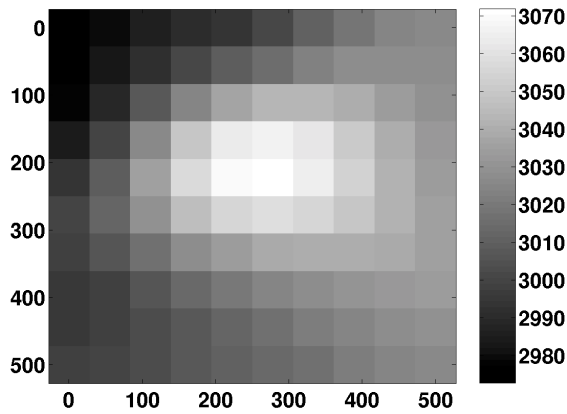


FIG. 6 Transmission tomography inversion result for model 3.

This result is also encouraging, though there is an acquisition imprint in the solution. The high velocity anomaly is present and has been smeared horizontally. The dominant raypath in a crosswell experiment is in the horizontal direction, leading to the smearing seen.

Reflection tomography

Using reflection tomography, the following results were obtained in attempting to invert for model 1. Figure 7 displays the velocity determined after three iterations.

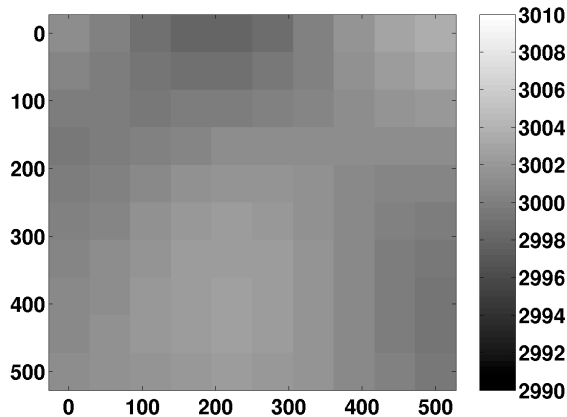


FIG. 7. Reflection tomography inversion result for model 1.

The solution converges nicely to a constant velocity model, comparable to the transmission experiment. Smoothing the velocity field after each iteration increases the rate of convergence for the constant velocity case as seen in the cross-well experiment.

Figure 8 shows the results in attempting to invert for model 2 after three iterations.

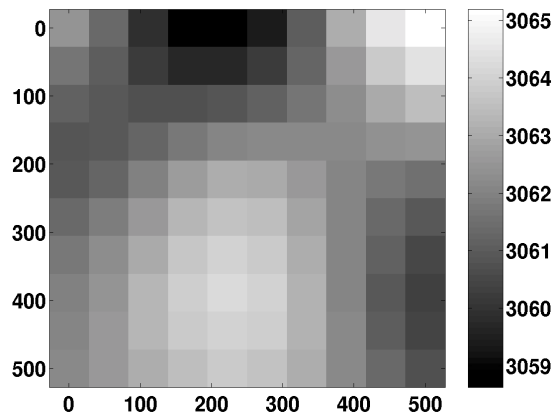


FIG. 8. Reflection tomography inversion result for model 2.

The above result demonstrates the inability of a surface reflection survey to detect a horizontal velocity anomaly mainly due to its acquisition geometry. There are no raypaths that traverse the model without passing through the high velocity layer. The inversion cannot detect any anomaly and presents a result with an average velocity of the model.

Figure 9 shows the results of the inversion for model 3.

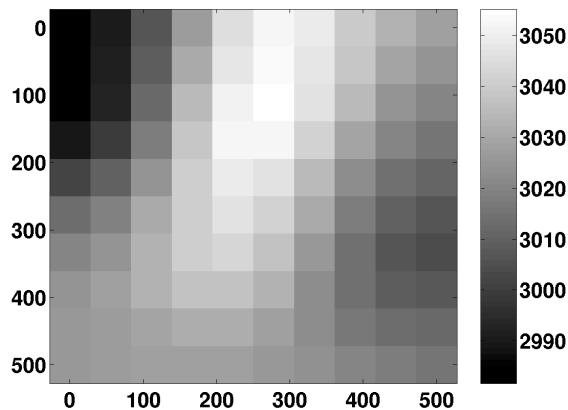


FIG. 9. Reflection tomography inversion result for model 3.

As seen in the cross-well experiment, the above figure demonstrates how the acquisition geometry distorts the velocity anomaly along the dominant travel path of the experiment. The residual error between the modelled and recorded traveltimes demonstrates the non-uniqueness present within tomography.

Integrated tomography

As seen in the previous figures, the tomographic solution is biased by the acquisition geometry. Combining two experiments using the quasi-null space as a reliability criterion the resultant velocity models show a marked improvement in determining the velocity model. This is not represented in the residual error since

tomography is a statistical method that attempts to minimize the residual error regardless of the final velocity model.

Using a null space threshold of 0.1 of the maximum singular value, the null spaces of the three models were computed for both reflection and transmission tomography. Figure 10 shows the null space for model 1.

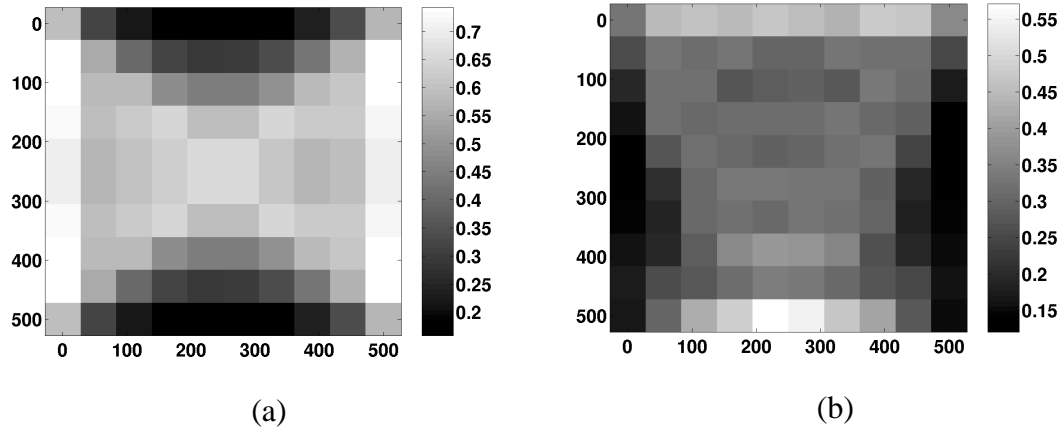


FIG. 10 Null space for the crosswell (a) and reflection (b) experiment of the constant velocity model. A higher quasi-null space value corresponds to a more reliable cell.

Figure 11 shows the integrated velocity model. This integrated model is a result of the combination of the well-constrained velocities of each section after one iteration of transmission and reflection tomography respectively. Alone, the edges of each survey are not as well constrained, but when combined, the surveys compliment each other and produce a superior tomogram.

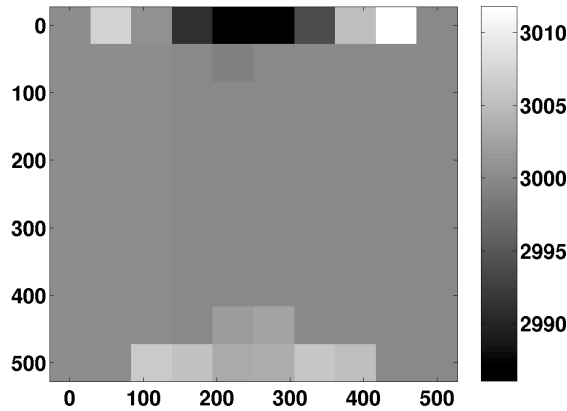


FIG. 11. Integrated constant velocity model.

Without any filtering applied, the resulting velocity model is a smooth solution accurately representing the actual velocity model. The upper and lower edges of the tomogram are the relatively poorly constrained areas of both the transmission and reflection tomography. In general, since reflection tomography determines the reflector position as well as the velocity, the reliability of each cell is less than the respective cell for the transmission experiment.

Figure 12 shows the null spaces for model 2.

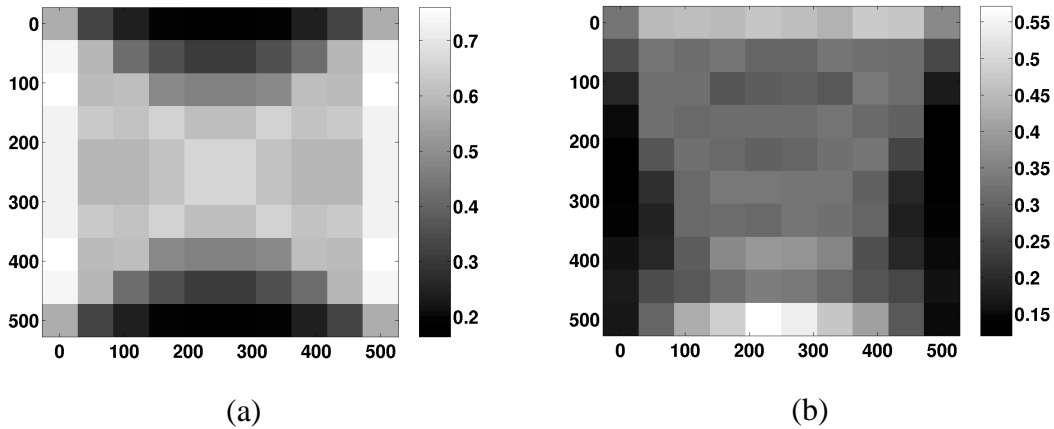


FIG. 12. Null space for the cross-well (a) and reflection (b) experiment of the horizontal velocity model. A higher quasi-null space value corresponds to a more reliable cell.

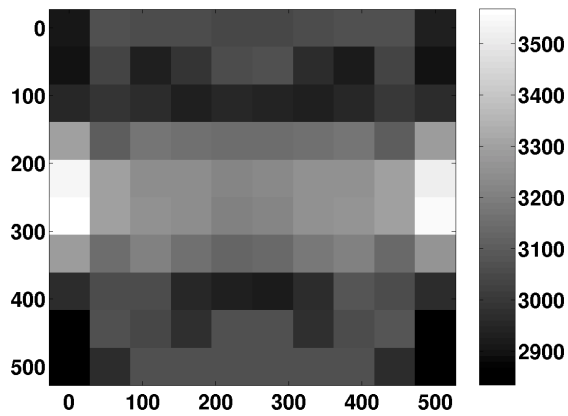


FIG. 13. Integrated velocity for model 2.

Comparing to the results of the reflection and transmission experiment, the integrated result is similar to the transmission tomography solution. The reflection survey does not detect the horizontal layer and the quasi-null space analysis was able to correctly determine solution reliability as demonstrated in the integrated result. This shows that there can be a measure of reliability assigned to each cell helping to build an accurate velocity model.

Figure 14 shows the null spaces for model 3.

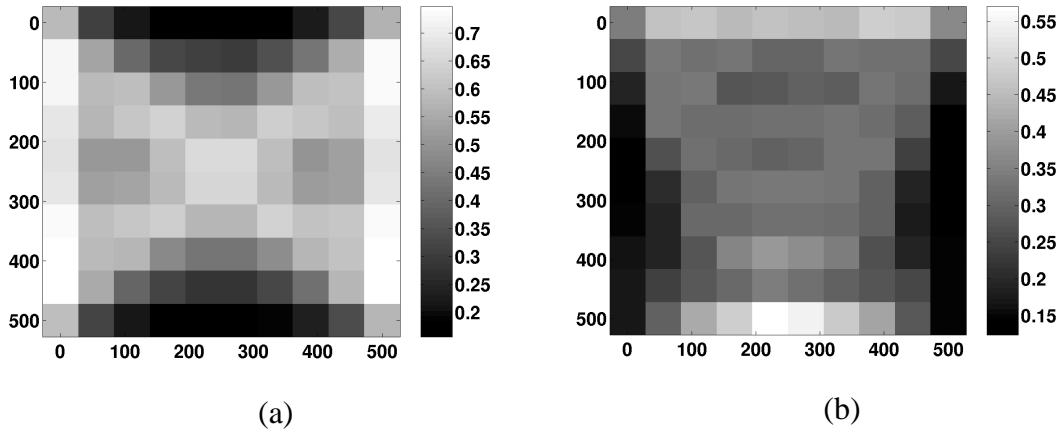


FIG. 14. Null space for the crosswell (a) and reflection (b) experiment of velocity model 3. A higher quasi-null space value corresponds to a more reliable cell.

Figure 15 shows the integrated velocity for model 3.

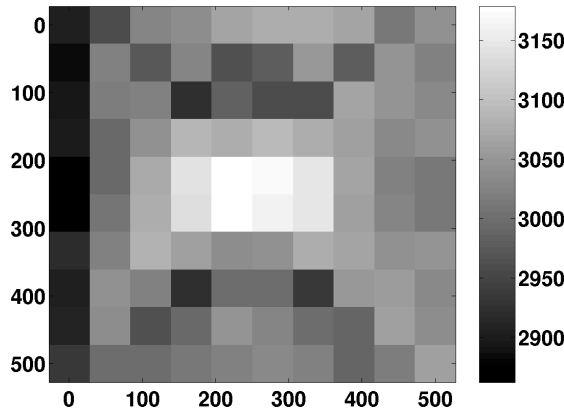


FIG. 15. Integrated velocity for model 3.

Figure 15 illustrates a more collapsed centre anomaly than is seen in either the reflection or transmission results. The smearing seen in the single experiments presents an ambiguity that is overcome using the quasi-null space analysis. A more resolved velocity model is determined by combining the well-constrained portions of each individual tomogram. Therefore mapping reliable and unreliable cells is an indication of whether the tomogram is accurately depicting the subsurface velocity structure.

Figures 16 through 18 show the residual error as a function of iteration number for models 1, 2, and 3. The residual errors are computed by summing the squares of the difference between the recorded and modelled traveltimes. Each figure contains four lines corresponding to the errors of transmission experiment, the reflection experiment and the error of the integrated solution inserted into the transmission and reflection experiment.

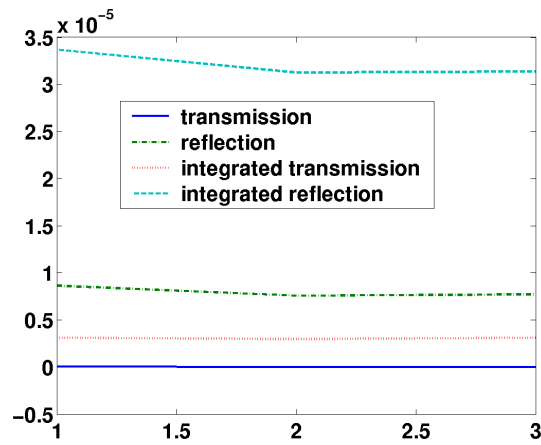


FIG. 16. Residual traveltimes for model 1.

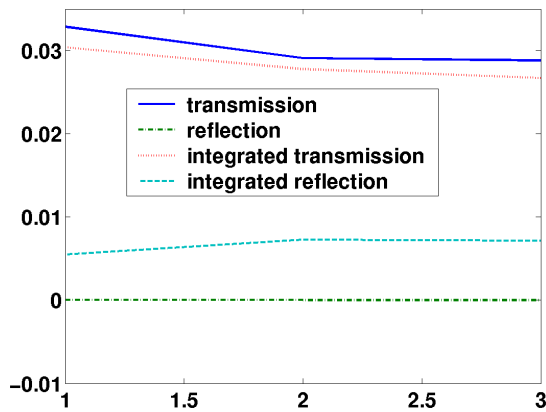


FIG. 17. Residual traveltimes for model 2.

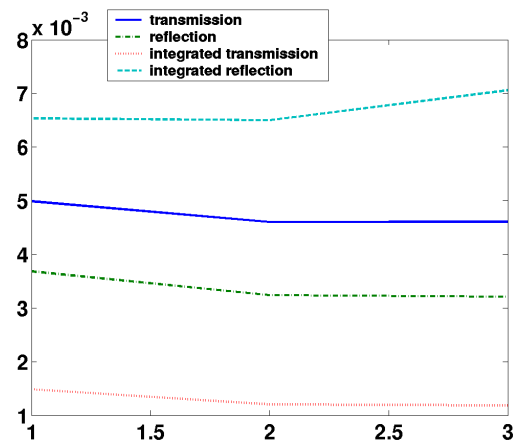


FIG. 18. Residual traveltimes for model 3.

The above figures demonstrate that the residual traveltimes are not always an accurate representation of velocity model correctness. The reflection tomography produces a model with very minimal residual error, however it does not accurately represent the actual velocity model. The quasi-null space is used as a tool to

overcome the solution ambiguity while still yielding acceptable residual traveltime errors.

CONCLUSION

The quasi-null space has been shown to be a powerful tool used to distinguish between well- and poorly constrained solutions. Examples of mapping the quasi-null space and integrating the well-constrained portions of two distinct experiments have been revealed more accurate solutions. The quasi-null space is able to overcome solution non-uniqueness and present better solutions even though the computed residual traveltime errors indicate otherwise. The integrated method provides a more reliable tomogram without a decrease in resolution and provides an accurate method for velocity model building.

ACKNOWLEDGEMENTS

The authors would like to thank the CREWES sponsors as well as Dr. Larry Lines and Shauna Oppert for useful discussions.

REFERENCES:

- Bishop, T., Bube, K., Cutler, R., Langan, R., Love, P., Resnick, J., Shuey, R., Spindler, D., and Wyld, H., 1985. Tomographic determination of velocity and depth in laterally varying media: *Geophysics*, **50**, 903-923.
- Bohm, G. and Vesnaver, A. L., 1999, In quest of the grid: *Geophysics*, **64**, 1116-1125.
- Carrion, P., 1991, Dual tomography for imaging complex structures: *Geophysics, Soc. of Expl. Geophys.*, **56**, 1395-1404.
- Lines, L.R. and LaFehr, E.D., 1989, Tomographic modeling of a cross-borehole data set: *Geophysics*, **54**, 1249-1257.
- Lines, L.R. and Treitel, S., 1984. Tutorial: A review of least-squares inversion and its application to geophysical problems: *Geophys. Prosp.*, **32**, 159-186.
- Perez, M.A. and Bancroft, J.C., 2000, Traveltime computation through isotropic media via the eikonal equation, *CREWES Research Report* **12**, 181-200.
- Perez, M.A. and Bancroft, J.C., 2001, Finite-difference anisotropic traveltimes and raypaths: *CREWES Research Report*, this volume
- Phillips, W.S. and Fehler, M.C., 1991, Traveltime tomography: A comparison of popular methods: *Geophysics, Soc. of Expl. Geophys.*, **56**, 1639-1649.
- Vesnaver, A., 1994, Towards the uniqueness of tomographic inversion solutions: *J. Seis. Expl.*, **3**, 323-334.
- Whitmore, N. and Lines, L., 1986, VSP depth migration of a salt dome flank: *Geophysics*, **51**, 1087-1109.